OVERVIEW OF THE NCNR ACCELERATOR STUDIES

Andrew J. Jason
Los Alamos National Laboratory
Los Alamos, NM 87545

I. INTRODUCTION

Since the construction of the Los Alamos Proton Storage Ring (PSR) [1], there has been a strong program for neutron research at the Manuel Lujan, Jr. Neutron Scattering Center (LANSCE). The PSR was designed to provide 80 kW of beam power to the LANSCE spallation target. In view of a possible upgrade for this facility, we have undertaken a study to delineate a system capable of delivering 1 MW of beam power to an upgraded LANSCE facility with provision for a further increase in power to 5 MW. The project is known as the National Center for Neutron Research (NCNR).

The concept emerging from these studies features acceleration of H^- ions to an energy of 800 MeV and subsequent multiturn injection into an accumulator ring. The compressed pulse is then extracted in a single turn and transported to the spallation target. In all the studies we have stressed reliability and low beam loss.

II. GENERAL DESCRIPTION

The proposed scheme is shown in Figure 1. The existing side-coupled linac (SCL), which accelerates beam from 100 MeV to 800 MeV and comprises about 90% of the LAMPF linac, is retained as an integral part of the proposal. The present front end consists of three ion sources that provide H^+, H^-, and polarized H^- accelerated by Cockroft-Walton generators to 750 MeV. The three beams are merged, bunched, and matched to a 201.25-MHz drift-tube linac (DTL) for acceleration to 100 MeV. Our concept replaces the three sources with a single H^- source capable of providing up to 40-mA peak current at 100 keV. Beam is then matched to a 402.5-MHz radio-frequency-quadrupole linac that bunches and accelerates beam to 7.0 MeV. The next stage of acceleration is provided by a 402.5-MHz DTL to 20 MeV and subsequent acceleration by an 805-MHz DTL to 100 MeV for matching into the 805-MHz SCL. The many choices in this specification involved considerations of beam dynamics, reliability, and cost. Additionally, the configuration can be upgraded in current by funneling into the 805-MHz DTL.

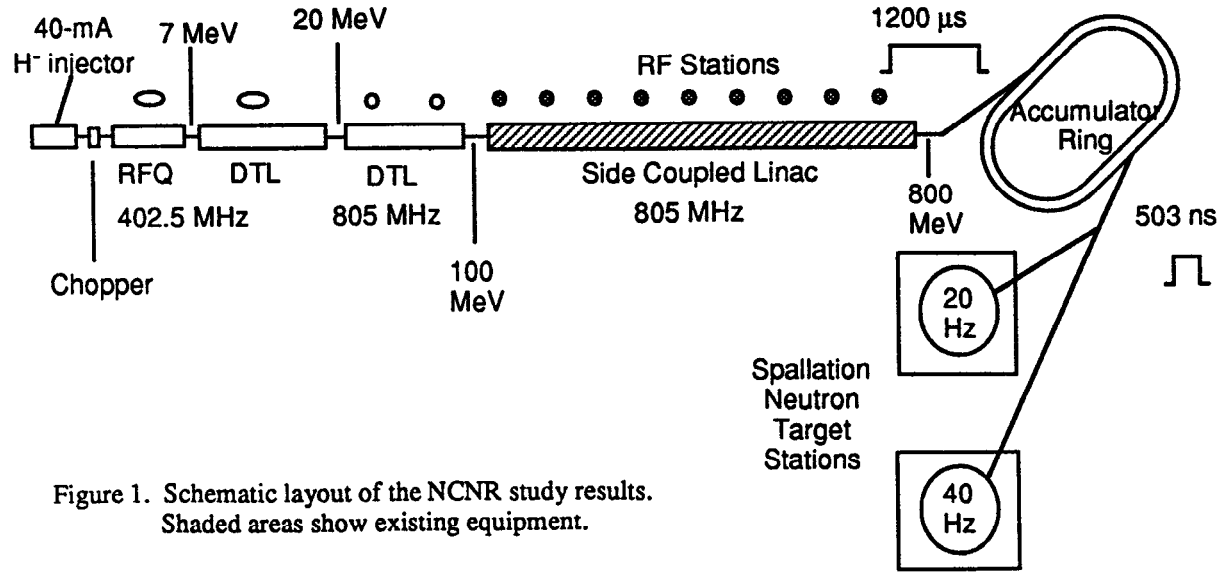

Figure 1. Schematic layout of the NCNR study results. Shaded areas show existing equipment.

*Work Supported by the US Department of Energy, Office of Defense Programs.

An achromatic transport line takes the beam northeast to the accumulator ring. The line also performs the function of dispersion scraping to remove off-momentum beam particles and contains magnets properly sized to avoid appreciable field stripping of the H^- beam. Beam is injected by single-stage stripping through a foil and, after accumulation for some 1790 turns, is immediately extracted. Beam is then transported to two spallation sources and inserted vertically upwards into the targets. Experiments at the neutron source generally require a regular pulse rate. Hence, pulsed equipment in the linac and ring must be capable of an 8.3-ms pulse repetition time to provide a uniform 20 and 40 Hz to the respective targets.

III. INJECTOR

Extensive development of high-current, high-brightness H^- ion sources has taken place at Los Alamos both for use at LAMPF [2] and for other projects such as the Ground Test Accelerator (GTA) [3]. We require currents near 40 mA with an rms normalized emittance of below 0.020π cm mrad and a duty factor near 9%. No existing ion source meets all these requirements although there are several applications for which one or more of the requirements has been exceeded. The 4X ion source developed for GTA has produced, for example, over 60 mA at about a third of the required emittance. However, the nominal duty factor for which it has been developed is 1%. The LAMPF ion source performs with adequate duty factor and emittance but produces a current of 20 mA. Similar comments also apply to sources developed at other institutions. With a modest development program, it is reasonable to extrapolate to the required performance.

A more difficult problem, for which no entirely satisfactory solution now exists, is that of chopping the beam at a 1.49-MHz rate (436 ns on, 235 ns off) to maintain an extraction gap in the compressor-ring stored beam. This is currently done for the PSR by a slow-wave deflector in the LAMPF injector region at 750-keV beam energy. Such a scheme will be difficult at the low-matching energy of the RFQ in the NCNR scheme. Several other options are being explored, among them fast beam switching at a source plasma electrode with modest pulsed-power requirements.

IV. LINAC

Specifications for the linac are given in Table 1

Table 1
Linac Parameters

Average current	1.4 mA
Average power	1.4 mA x 800 MeV=1.12 MW
Peak current	30 mA
Repetition rate	20 + 40 Hz
Beam duty factor	7.2 %
Macropulse length	1.2 ms
Micropulse frequency	402.5 MHz
Chopping frequency, duty factor	1.49 MHz, 65%

The RFQ selected is similar to previous four-vane designs constructed or proposed at Los Alamos [4]. The high output energy of 7 MeV requires an unusual length of 6.9 m. The RFQ features an integral copper vacuum, rf, and structural envelope and is constructed in eight electroformed sections. Each pair of sections forms a loop-driven rf segment resonantly coupled to the others in a coupled-cavity structure. The average structure power is 140 kW with a peak power (including beam) of 1.54 MW. Proven tuning algorithms have been developed for this type of device. Dynamics calculations show that the structure will have over 95% transmission with an emittance of 0.02π cm mrad (rms normalized) at 38 mA.

The 402.5-MHz DTL is designed with two tanks and a total length of 5.43 m. Permanent-magnet quadrupoles are used in an FFDD configuration. Drift-tube bores are 1.8-cm diameter, approximately 10 times rms beam size. The DTL is similar to designs tested at Los Alamos on GTA and other projects. The total peak power needed is 1.48 MW. This is to be supplied by a two-tube klystron module with each tube providing a nominal 1.25 MW of rf peak power. Beam-dynamics calculations show little emittance growth with a test current of 38 mA.

The 805.0-MHz DTL is similarly constructed with a total length of 54.7 m and consists of 15 tanks. The lattice is a FFFOOODDDOOO configuration using 1.8-cm-bore permanent-magnet quadrupoles. From our loss estimates and extensive testing of magnetic material, we do not believe that radiation-induced deterioration of the magnets will be appreciable over a period of many years. The ratio of aperture radius to beam rms size is greater than the factor of seven generally used at LAMPF as a "safe" value. Beam-dynamics calculations show small emittance growth with a current of 75 mA. The total peak rf power required is 5.8 MW to be supplied by a klystron module similar to that used for the 402.5-MHz DTL.

Matching between the four linac sections is done transversely with variable permanent-magnet quadrupoles and longitudinally with pairs of buncher cavities. The buncher systems require a total of 50-kW peak power and are supplied by six tetrode-driven supplies.

Studies and experimental results have shown that the LAMPF SCL (100 to 800 MeV) is quite adequate for NCNR purposes. Note that the LAMPF facility has functioned as a provider of beam at 1-MW levels at a repetition rate of 120 Hz with a micropulse frequency of 201.25 MHz. At these levels, it operates under low stress and has had a long history of high reliability. Our proposal nearly doubles the peak current. However, the increase in micropulse frequency to 402.5 MHz results in a similar charge per beam bunch; the single-bunch beam dynamics is hence unchanged. Because of the 65% chopping duty factor, the peak-average current is 19.5 mA, slightly above the present nominal current of 17 mA. Total peak power is then nearly 41 MW, to be supplied by the existing 44-klyston system. Taking into account the ratio of total supplied power to structure losses (~4/3), the additional average power to be supplied is some 4%, well within the present rf-system reserve capacity. Hence, no substantial upgrade is needed.

A remaining question is the SCL response to the chopping pattern. Beam to the PSR is currently supplied at about one-third the NCNR peak-current requirement and at twice the chopping frequency with no perceived perturbation to performance. Combined structure and beam-dynamics calculations show that, under NCNR conditions, the cavity fields will vary uniformly in each tank by about 1% during the chopping cycle but will have little effect on beam quality. This point will be tested in an upcoming series of experiments.

Recent advances in fast adaptive feed-forward control techniques [7], proven on operating systems, will be very useful in achieving low-loss beam control in the linac and will soon be tested on the SCL. Studies are underway for high-current adaptations to tuning techniques such as the Δt method. Programs are also in place to study halo growth and develop techniques that minimize beam loss [8].

V. ACCUMULATOR RING

A. Overview

The linac chopping pattern is superimposed on the stored beam by direct non-Liouvillean injection through a foil. Transverse injection painting is used to control the beam distribution, important for the ring stability. A gap is maintained by an rf system consisting of twelve cavities operating at first through fifth ring harmonic to produce a barrier bucket. At extraction, the gap is 168 ns, sufficient for a fast ferrite kicker to rise and cleanly remove the 503-ns beam bunch from the ring in single-turn extraction.

A ring closed-orbit energy of 790.0 MeV was chosen, slightly less than the nominal 800 MeV delivered by the accelerator, in order to provide for an energy sweep of ±4 MeV during injection. The ring circumference of 168.886 m was chosen so that the revolution frequency for 790-MeV protons is a subharmonic of 805 MHz; additionally, all five barrier-bucket rf harmonics are subharmonics of 805 MHz. A barrier bucket was chosen for its ability to keep the extraction gap free of protons (assuming successful chopping), avoiding extraction losses as well as a possible electron-proton instability. Additionally, the barrier bucket allows maximum beam capture and provides a bunching factor of 0.55 as compared to 0.25 for a first-harmonic cavity. The beam emittance necessary to keep the space-charge tune depression below a certain value is inversely proportional to the bunching factor.

Major design parameters are given in Table 2 and a schematic layout is shown in Figure 2.

Table 2
Accumulator-Ring Parameters

Ring circumference	168.886 m
Accumulated turns	1790
Ring period	671 ns
Extracted-beam-bunch length	503 ns
Stored protons	1.3×10^{14}
Peak stored current	57 A
Average extracted current	1.25 mA
Number of cells in achromatic arc	4
Number of cells in straight section	5
Length of straight-section cell	10.407 m
Length of arc cell	8.1 m

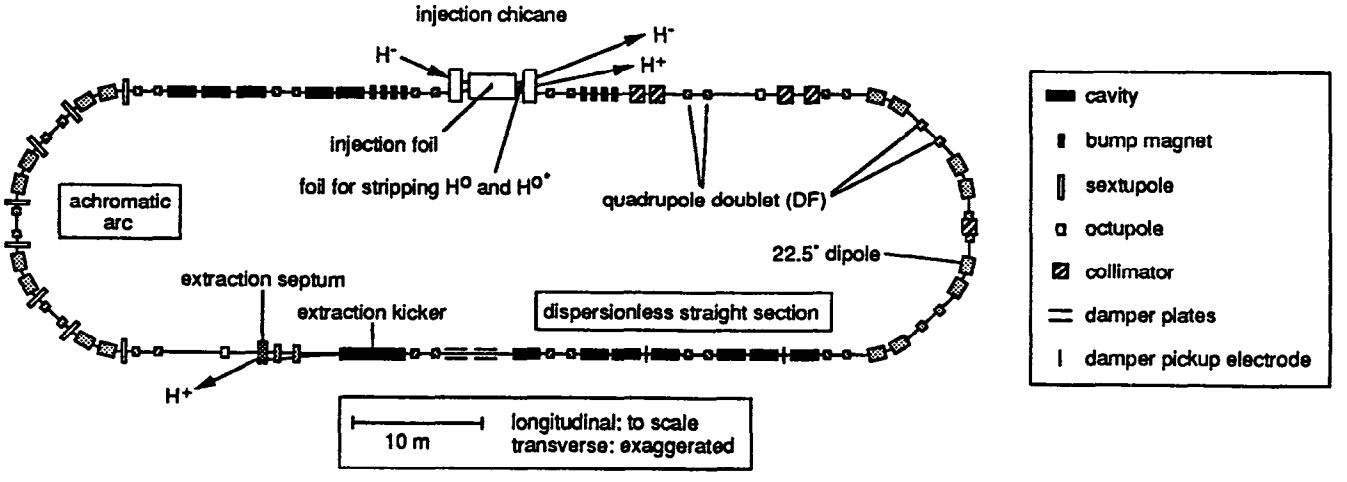

Figure 2. Ring layout

The ring features dispersionless straight sections and arcs in the configuration of second-order achromats. Straight sections house the injection chicane, bump magnets for injection painting, collimators for beam-halo control, bunching cavities, a transverse-damper system, linear and nonlinear corrector elements, and the extraction kicker and extraction septum. One achromatic arc houses chromaticity-adjusting sextupoles, the other a dispersion collimator. A full complement of diagnostics and orbit-correction steerers are included.

The desire to accomplish injection in a single drift mandated a minimum drift length of 8 m. This, together with the achromatic-arc design, suggested a doublet as opposed to a singlet lattice. Five cells per straight section were chosen because of tune considerations, because for the required ring circumference the long drifts are adequately dimensioned (8.407 m), and because the five long drifts in low-loss areas (upstream of the injection chicane and extraction kicker) can hold all rf cavities.

B. Linear Lattice

The lattice functions of the ring, slightly different from those of one superperiod because of the injection chicane, are shown in Figure 3. The undepressed tunes, $Q_x = 4.23$, $Q_y = 5.19$, correspond to phase advances per straight-section cell of 80.28° and 114.84°, respectively, near the value of 90° that minimizes aperture requirements. Stored-beam emittances are $\varepsilon_x = \varepsilon_y = 110\pi$ mm mrad to limit space-charge tune shifts to -0.15, thus remaining in a stable region of tune space. Apertures are dimensioned for transverse acceptances of 420π mm mrad and a momentum acceptance of ±1% $\delta p/p$. Ring dipoles and quadrupoles are described in Table 3.

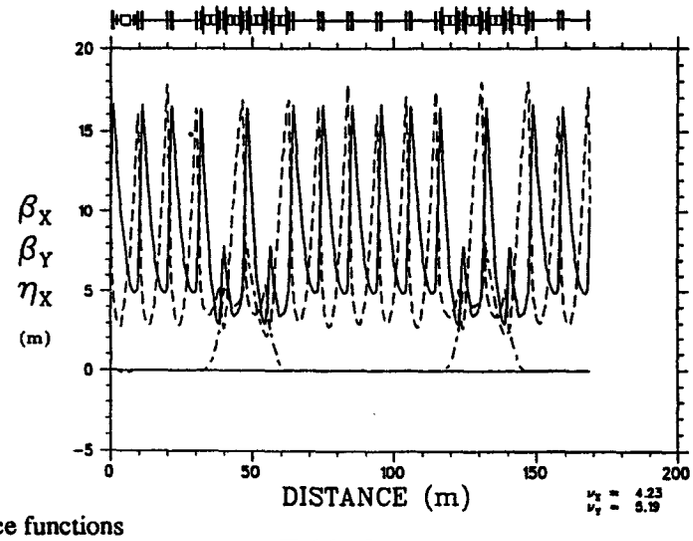

Figure 3. Ring lattice functions

Table 3
Ring-Magnet Description

Dipoles	
Arc length (m)	1.600
Field (T)	1.188
Straight-Section Quadrupoles	0.500
Defocusing-QuadrupoleGradient(T/m)	-4.541
Focusing Quadrupole Gradient (T/m)	3.990
Achromatic-Arc Quadrupole	
Effective Length (m)	0.500
Defocusing-Quadrupole Gradient (T/m)	-3.687
Focusing-Quadrupole Gradient (T/m)	4.366

C. Nonlinear Issues

The natural first- and second-order chromaticities and the anharmonicities for the perfect ring, without either random or systematic errors in the magnetic elements, are given in Table 4. The beam will cover a large area in the tune diagram, both from the tune shift of the reference particle due to space charge, and the tune spread around the central value, due to chromaticities and anharmonicities. Two families of four sextupoles each are placed in one arc to affect chromaticities. Two octupoles are placed at identical positions in the two superperiods to affect anharmonicities for control of tune spread.

Table 4
Nonlinear Ring Parameters

$\partial Q_x / \partial(\delta p/p)$	-4.86
$\partial Q_y / \partial(\delta p/p)$	-7.10
$\partial^2 Q_x / \partial(\delta p/p)^2$	182.07
$\partial^2 Q_y / \partial(\delta p/p)^2$	120.69
$\partial Q_x / \partial \varepsilon_x$ $(\pi$ m rad$)^{-1}$	31.79
$\partial Q_y / \partial \varepsilon_y$ $(\pi$ m rad$)^{-1}$	34.49
$\partial Q_x / \partial \varepsilon_y = \partial Q_y / \partial \varepsilon_x$ $(\pi$ m rad$)^{-1}$	42.97

Adjustment of the tune spread by these methods and by shaping the beam distribution are means of controlling the ring stability via tune damping. If a large tune spread is maintained, the damper shown in Figure 2 may not be necessary or useful since the decoherence time will be small. Calculation of the form factors and impedances involved in a complete stability assessment is difficult and has not yet been accomplished. However, we now argue for ring stability by scaling from other rings, such as the PSR for which form factors and impedances are scalable, that have not shown a particular instability at a given charge-storage level. The PSR does, however, exhibit an electron-proton instability [10] which we believe can be avoided by keeping the extraction gap free of protons, by loss control, and by the possible implementation of clearing electrodes. Experiments are underway to assess some of these issues at the PSR.

The widths of the resonance lines in the presence of ring imperfections, such as quadrupole roll errors, and random and systematic higher-multipole errors in dipole and quadrupole fields, are a concern. Sets of Lambertson correctors are placed inside straight-section quadrupoles to affect the widths of resonance lines. Skew-quadrupole correctors to affect $Q_x - Q_y = 1$, normal-octupole correctors to affect $4Q_x = 17$, and normal-decapole correctors to affect $Q_x + 4Q_y = 25$, $3Q_x + 2Q_y = 23$ and $5Q_x = 21$ have been identified.

D. Ring Injection

The injection chicane, composed of two 5° septa and a 10° central dipole, moves the stored-beam orbit outward by 0.2 m. The injected H^- join the stored-beam orbit outward by 0.2 m. Unstripped H^- are deflected away from the stored beam and disposed of in a beam dump, causing minimal activation in the ring. Partially-stripped excited neutral atoms created by the foil stripping process have been identified as a source of activation [9] in the PSR. These excited atoms are stripped in the fringe field of a downstream magnet and are scattered by the field to outside the ring acceptance. It is possible in principle to reduce these losses from a few percent of the injected beam to $<10^{-5}$ by placing the stripper foil in a specially configured magnetic field.

Injection occurs in a nondispersive region; hence the painting process is uncoupled from beam momentum. Two independent sets of bump magnets relax the stored-beam centroid from near the injection point (e.g., ~2.5 cm, -4.0 mrad in the x plane) to the closed orbit during injection. Thus the initial bump coordinates define the final stored-beam emittance. The nominal bumping rate is adjusted so that the stored emittance grows linearly in time. The foil, configured as a small rectangle and supported by 5-micron carbon fibers, is positioned so that its corner just covers the injected beam. Injection painting keeps the number of foil traversals low, at an average of 10 per particle. Figure 4 shows a contour plot of the beam transverse distribution at the end of injection, assuming accumulation in the perfect ring and neglecting beam self-interaction. Because of the x-y correlation inherent in this bumping scheme, the distribution is rectangular and the X-shaped pileup noticeable in the figure engenders space-charge forces with octupolar components.

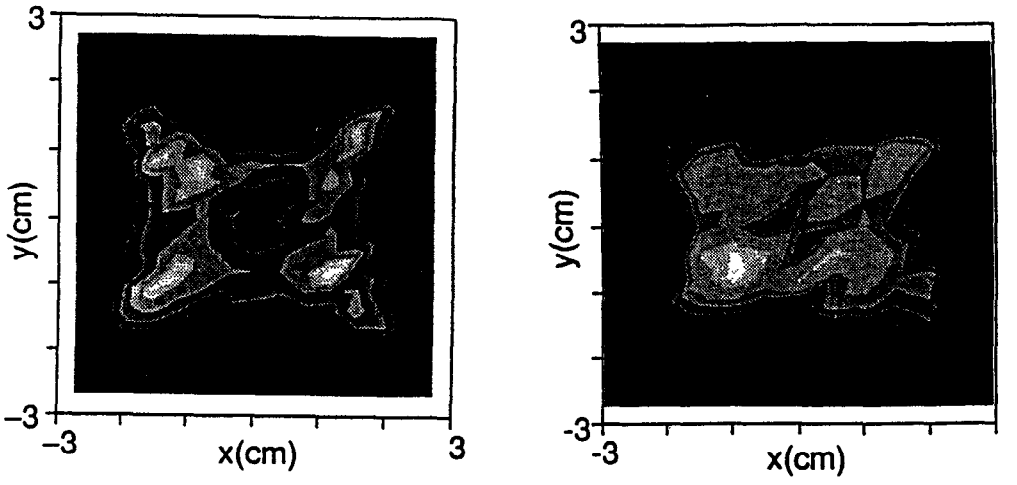

Figure 4. Left, transverse beam distribution after injection with neglect of space-charge forces. Right, evolution of this distribution for 100 turns including the forces derived from the distribution potential.

E. Particle Tracking

Figure 4 also indicates the effect of space charge forces. In the right-hand diagram the beam potential was calculated for the distribution on the left in the form of a fourth-order polynomial. Particles were then tracked with the high-order code Marylie for 100 turns. The resultant distribution shown is smoother and has slighty increased in size. Efforts are underway for a more self-consistent tracking capability.

The machine dynamic aperture was assessed by single-particle tracking to ninth order with the beam-optics code Tlie. We assumed random quadrupole-roll errors with a 10-mrad rms distribution, random sextupole errors of 0.01 T/m^2 rms and decapole errors of 1.0 T/m^4 rms in the dipoles, and octupole errors of 0.05 T/m^3 rms in the quadrupoles. The dynamic aperture as a function of particle momentum is shown in Figure 5. This strange looking diagram shows the fractal like nature of the nonlinear forces; were we to increase the resoulution, contours would further decrease in regularity. Improvements to the dynamic aperture will be made using first- and higher-order corrector elements.

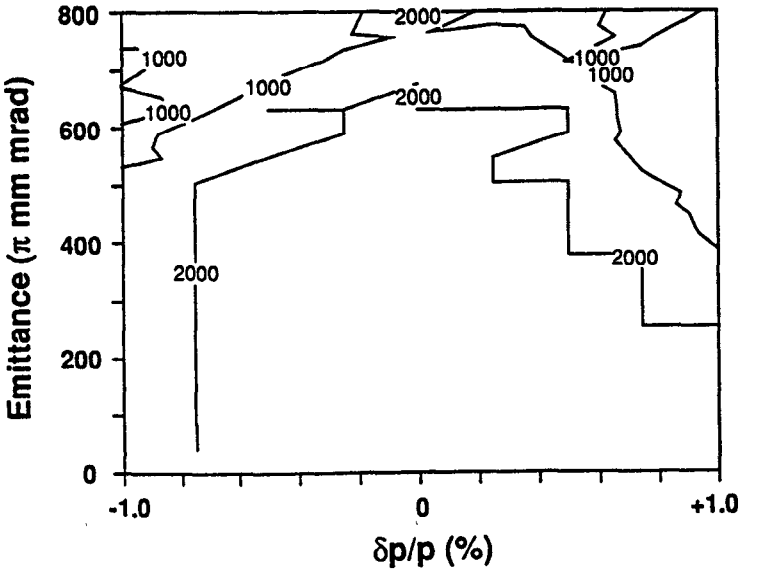

Figure 5. Contour plots for particles remaining within the emittance aperture on the vertical axis for 1000 and 2000 turns as a function of relative momentum deviation from the nominal. The particles were originally placed on the linear emittance contour corresponding to the ordinate value. Those particles that did not remain for the specified number of turns left the machine.

VI. UPGRADE OPTIONS

Although the major thrust of our study has been toward the 1-MW scenario, several options have been proposed for an upgrade to 5 MW and we have included features needed by these options in our design. The new linac front end is highly adaptable to funneling for increasing the current by the needed factor of 5 if a final energy of 800 MeV is retained. In this case further work is needed to establish the current-carrying capacity of the SCL and a multiple ring system would be needed.

The alternative, a higher beam energy of up to 2 GeV, is very attractive. Here a single ring, but with a substantially different lattice, appears feasible. Replacement of the CCL with a superconducting linac would use the existing LAMPF infrastructure and would ensure insensitivity to the chopping pattern that poses problems for a low-stored-energy room-temperature structure. Studies on upgrade alternatives are continuing.

VII. ACKNOWLEDGMENTS

We wish to thank the many individuals from LANSCE and AT and MP Divisions who contributed to this study.

VI. REFERENCES

[1] G. P. Lawrence, R. A. Hardekopf, A. J. Jason, P. N. Clout and G. A. Sawyer, "Los Alamos High-Current Proton Storage Ring; a Status Report," *IEEE Trans. Nucl. Sci.* NS-32, No. 5, 2662 (1985).

[2] R. York, D. Tupa, and D. Swenson, "Volume H^- Source Development at LAMPF," to be published in the Proceedings of the 1993 IEEE Particle Accelerator Conference.

[3] H. V. Smith, J. D. Sherman, P. Allison, "Pulsed H^- Ion Beams from Penning SPS Sources Equipped with Circular Emitters," *Proceedings of the 1988 Linear Accelerator Conference*, Newport News, October, 1988, p 164.

[4] L. Young, "Segmented Resonant Coupled Radio Frequency Quadrupole," these proceedings.

[5] K. Johnson, et al., "Commissioning of the First Drift Tube Linac Module in the Ground Test Accelerator," to be published in the Proceedings of the 1993 IEEE Particle Accelerator Conference.

[6] M. Lynch, et al., "Linac Design Study for an Intense Neutron-Source Driver," to be published in the Proceedings of the 1993 IEEE Particle Accelerator Conference.

[7] C. D. Ziomek, "Adaptive Feedforward in the LANL RF Control System," *Proceedings of the 1992 Linear Accelerator Conference*, Ottowa, August, 1992, p 685.

[8] R. Jameson, "Design for Low Beam Loss in Accelerators for Intense Neutron Applications," to be published in the Proceedings of the 1993 IEEE Particle Accelerator Conference.

[9] R. Hutson, R. Macek, "First-Turn Losses in the LAMPF Proton Storage Ring (PSR)," to be published in the Proceedings of the 1993 IEEE Particle Accelerator Conference.

[10] T. S. Wang, et al, "Recent Study of Beam Stability in the PSR," to be published in the Proceedings of the 1993 IEEE Particle Accelerator Conference.